Light-Controlled Self-Assembly of Semiconductor Nanoparticles into Twisted Ribbons

Sudhanshu Srivastava, *et al.*

Science **327**, 1355 (2010);
DOI: 10.1126/science.1177218

References and Notes

1. H. J. Kimble, *Nature* **453**, 1023 (2008).
2. T. Wilk, S. C. Webster, A. Kuhn, G. Rempe, *Science* **317**, 488 (2007).
3. J. M. Raimond, M. Brune, S. Haroche, *Rev. Mod. Phys.* **73**, 565 (2001).
4. H. Häffner, C. F. Roosa, R. Blatt, *Phys. Rep.* **469**, 155 (2008).
5. A. Wallraff *et al.*, *Nature* **431**, 162 (2004).
6. J. M. Gérard *et al.*, *Phys. Rev. Lett.* **81**, 1110 (1998).
7. K. Hennessy *et al.*, *Nature* **445**, 896 (2007).
8. I. Fushman *et al.*, *Science* **320**, 769 (2008).
9. Y. Akahane, T. Asano, B.-S. Song, S. Noda, *Nature* **425**, 944 (2003).
10. P. W. Anderson, *Phys. Rev.* **109**, 1492 (1958).
11. D. S. Wiersma, P. Bartolini, A. Lagendijk, R. Righini, *Nature* **390**, 671 (1997).
12. H. Hu, A. Strybulevych, J. H. Page, S. E. Skipetrov, B. A. van Tiggelen, *Nat. Phys.* **4**, 945 (2008).
13. J. Billy *et al.*, *Nature* **453**, 891 (2008).
14. J. Topolancik, B. Ilic, F. Vollmer, *Phys. Rev. Lett.* **99**, 253901 (2007).
15. T. Lund-Hansen *et al.*, *Phys. Rev. Lett.* **101**, 113903 (2008).
16. E. Knill, R. Laflamme, G. J. Milburn, *Nature* **409**, 46 (2001).
17. S. Hughes, L. Ramunno, J. F. Young, J. E. Sipe, *Phys. Rev. Lett.* **94**, 033903 (2005).
18. S. John, *Phys. Rev. Lett.* **58**, 2486 (1987).
19. A. F. Koenderink, A. Lagendijk, W. L. Vos, *Phys. Rev. B* **72**, 153102 (2005).
20. S. Mazoyer, J. P. Hugonin, P. Lalanne, *Phys. Rev. Lett.* **103**, 063903 (2009).
21. A. A. Chabanov, M. Stoytchev, A. Z. Genack, *Nature* **404**, 850 (2000).
22. J. Topolancik, F. Vollmer, B. Ilic, *Appl. Phys. Lett.* **91**, 201102 (2007).
23. Materials and methods are available as supporting material on *Science* Online.
24. A. Lagendijk, B. van Tiggelen, D. S. Wiersma, *Phys. Today* **62**, 24 (2009).
25. B. Shapiro, *Phys. Rev. Lett.* **83**, 4733 (1999).
26. V. S. C. Manga Rao, S. Hughes, *Phys. Rev. B* **75**, 205437 (2007).
27. P. Lodahl *et al.*, *Nature* **430**, 654 (2004).
28. R. C. Somers, M. G. Bawendi, D. G. Nocera, *Chem. Soc. Rev.* **36**, 579 (2007).
29. J. B. Pendry, *J. Phys. C* **20**, 733 (1987).
30. J. Bertolotti, S. Gottardo, D. S. Wiersma, M. Ghulinyan, L. Pavesi, *Phys. Rev. Lett.* **94**, 113903 (2005).

31. We gratefully acknowledge T. Schlereth and S. Höfling for quantum dot growth, J.M. Hvam for discussions, and the Council for Independent Research (Technology and Production Sciences and Natural Sciences) and the Villum Kann Rasmussen Foundation for financial support.

Supporting Online Material

www.sciencemag.org/cgi/content/full/327/5971/1352/DC1
Materials and Methods
References

24 November 2009; accepted 20 January 2010
10.1126/science.1185080

Light-Controlled Self-Assembly of Semiconductor Nanoparticles into Twisted Ribbons

Sudhanshu Srivastava,[1] Aaron Santos,[1] Kevin Critchley,[1,2] Ki-Sub Kim,[1,3] Paul Podsiadlo,[1,4] Kai Sun,[5] Jaebeom Lee,[1,7] Chuanlai Xu,[1,8] G. Daniel Lilly,[1] Sharon C. Glotzer,[1,6]* Nicholas A. Kotov[1,5,6,7]*

The collective properties of nanoparticles manifest in their ability to self-organize into complex microscale structures. Slow oxidation of tellurium ions in cadmium telluride (CdTe) nanoparticles results in the assembly of 1- to 4-micrometer-long flat ribbons made of several layers of individual cadmium sulfide (CdS)/CdTe nanocrystals. Twisting of the ribbons with an equal distribution of left and right helices was induced by illumination with visible light. The pitch lengths (250 to 1500 nanometers) varied with illumination dose, and the twisting was associated with the relief of mechanical shear stress in assembled ribbons caused by photooxidation of CdS. Unusual shapes of multiparticle assemblies, such as ellipsoidal clouds, dog-bone agglomerates, and ribbon bunches, were observed as intermediate stages. Computer simulations revealed that the balance between attraction and electrostatic repulsion determines the resulting geometry and dimensionality of the nanoparticle assemblies.

Spirals, helicoids, helices, twisted ribbons (TRs), and other helical structures present fascinating geometries from the perspectives of mathematics, biology, optics, and mechanics. The formation of helices from nanoparticles (NPs) will make possible exploitation of the unusual properties of helices arising from quantum confinement (*1*, *2*) within NPs, as well as expand the design space (*3*, *4*) and offer new means of controlling the pitch and/or chirality of the helical structures. To achieve self-organization of such intricate objects, it is necessary to fine-tune the overall balance of forces, including anisotropy of interactions that drive assembly of NPs into larger structures. Control of these processes will require the discovery of many-body interactions at the nanoscale, as well as understanding their dynamics and capabilities of formation of complex self-organized patterns transitioning from nano- to microscale.

As a model system for realizing these goals, we used an aqueous dispersion of CdTe (*5*) NPs (emission maximum at 550 nm) prepared (*6*) with thioglycolic acid (TGA) as a stabilizer with the TGA-to-Cd^{2+} ratio close to 1.0, rather than the traditional value of 2.4 (*7*). Based on the variety of existing data (*1*, *6*, *8*), these NPs exhibit strong anisotropy due to permanent dipoles on them (*1*, *8*). The strongly reduced concentration of TGA is expected to lead to the elimination of tetrahedral apices, where the local concentration of TGA is the highest, and an increase of the average value of dipole on NPs. It also increases chemical reactivity of the NPs, which intricately interplays with the interparticle forces. After preparation, the CdTe NPs are precipitated by addition of methanol and centrifuged for 20 min, followed by redispersion in deionized water at pH = 9 (adjusted by addition of NaOH). The orange color of the NP solution turns dark green within ~72 hours, indicating that NP self-assembly has occurred.

TRs with distinctive helicity (Fig. 1, A, B, and D to F), were the primary product of the aging process (Fig. 1) (*6*). The length of the TRs made from CdTe typically ranged from 0.8 to 2 μm, but can be as long as 8 μm (Fig. 1). Some straight nanowires (NWs) were also produced as a secondary product (Fig. 1C) and were identified as well-studied single crystalline Te wires (fig. S1) (*7*). Unlike these NWs or other NP assemblies (*6*), the TRs were made from individual NPs layered on top of each other (Fig. 1, G to I). Their thickness, as determined by atomic force microscopy (AFM), was 10 to 12 nm and corresponds to three to four NP layers. The pitch of the CdTe TRs averaged ~350 nm (Fig. 1, E and F). The distribution between right- and left-handed twisting was approximately equal: 52% right and 48% left, which indicates a nearly racemic mixture of chiral isomers (fig. S2) (*7*). Remarkably, the helical ribbons form bundles in which all TRs have the same chirality. Instead of the typical red shift of optical features found in previous studies of NP assemblies (*6*, *9*, *10*), a gradual blue shift of the luminescence and absorption peaks was observed during formation of TRs (Fig. 2A). This observation normally would have indicated the decrease in delocalization volume of excitons in CdTe and, hence, a wholly different process is taking place than that previously reported. This phenomenon is rather unusual but can be understood when the entire process of transformation of NPs to helicoidal structures is discussed.

We first characterized the composition of the products with x-ray energy dispersive spectroscopy (XEDS). The atomic percent Cd:Te:S ratio for TRs and original CdTe NPs was 46:10:44 and 43:38:19, respectively. The assembly process is associated with considerable loss of Te and transition to CdS/CdTe NPs, in which the CdS phase is strongly dominant. This substantial change of

[1]Department of Chemical Engineering, University of Michigan, Ann Arbor, MI 48109, USA. [2]School of Physics and Astronomy, University of Leeds, Leeds LS2 9JT, UK. [3]Department of Chemical and Biological Engineering, Chungju National University, 72 Daehak-ro, Chungju, Chungbuk 380-702, Republic of Korea. [4]Center for Nanoscale Materials, Argonne National Laboratory, Argonne, IL 60439, USA. [5]Department of Materials Science and Engineering, University of Michigan, Ann Arbor, MI 48109, USA. [6]Department of Biomedical Engineering, University of Michigan, Ann Arbor, MI 48109, USA. [7]Department of Nanomedical Engineering, College of Nanoscience and Nanoengineering, Pusan National University, Miryang 627-706, Republic of Korea. [8]School of Food Science and Technology, Jiangnan University, Wuxi, Jiangsu 214122, China.

*To whom correspondence should be addressed. E-mail: sglotzer@umich.edu (S.C.G.); kotov@umich.edu (N.A.K.)

the composition can be observed in high-resolution transmission electron microscopy (HRTEM) images (Fig. 2, C and D). The lattice spacing for {111} planes for as-prepared CdTe NPs is 0.384 nm but is shorter for NPs in TRs: 0.344 nm (Fig. 2C), as expected for CdS particles. Selected-area electron diffraction (SAED) patterns of the TRs showed the presence of characteristic diffraction patterns for both CdTe (111) (d = 0.38 nm), (220) (d = 0.22 nm), and CdS (100) (d = 0.34 nm), (101) (d = 0.31 nm), and (110) (d = 0.19 nm) planes (*11*) (Fig. 2, E and F). These data and the presence of Te NWs indicate that the process of oxidation Te^{2-} to Te^{0} takes place.

To gain better knowledge about the transformation of NPs into TR, dynamics of multiparticle assembly, and driving forces of this process, we investigated the intermediate stages of

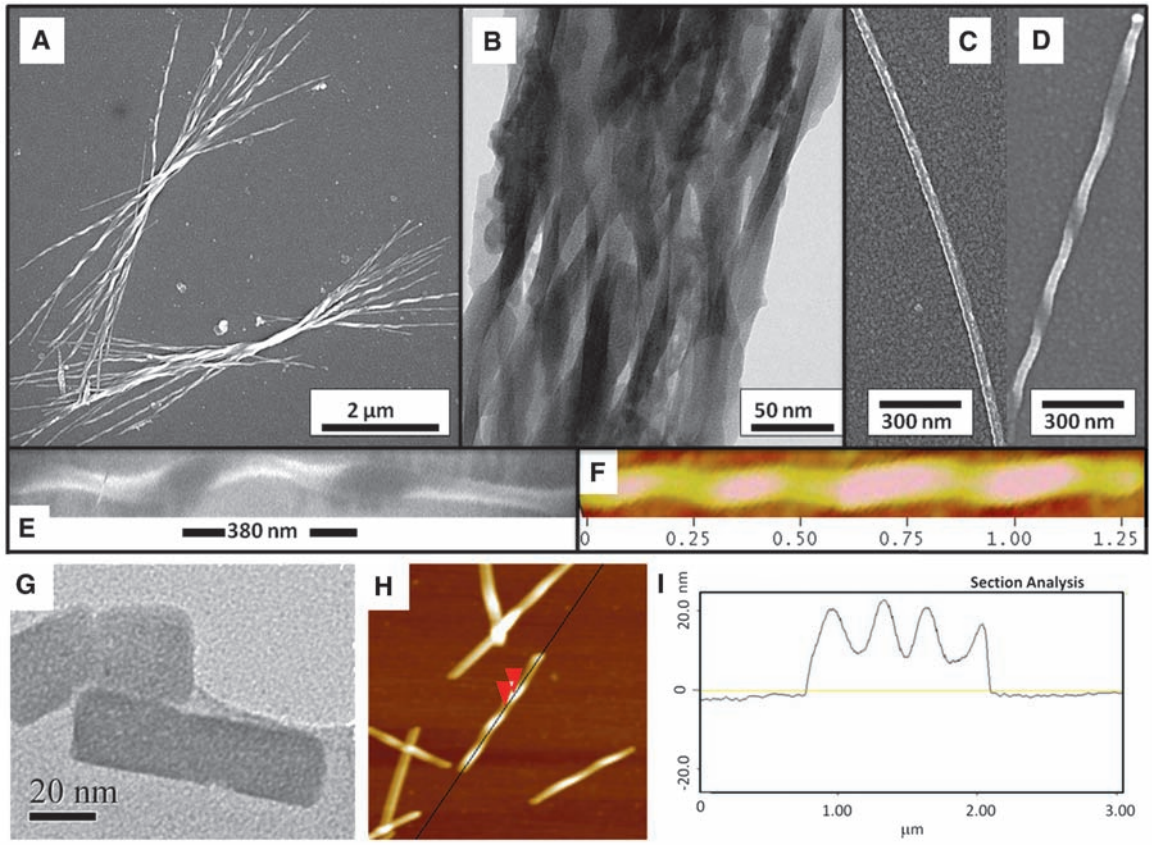

Fig. 1. (**A** and **B**) SEM (A) and TEM (B) images of bundles of TRs. (**C** and **D**) Individual straight Te NWs (C) and CdTe/CdS TRs (D). (**E** and **F**) SEM (E) and AFM images (F) of individual TRs with pitch lengths of 380 (E) and 400 nm (F). (**G**) TEM image of a cross section of TRs (the cutting plane may not be perpendicular to the TR axis). (**H** and **I**) AFM image and cross-sectional analysis of TRs.

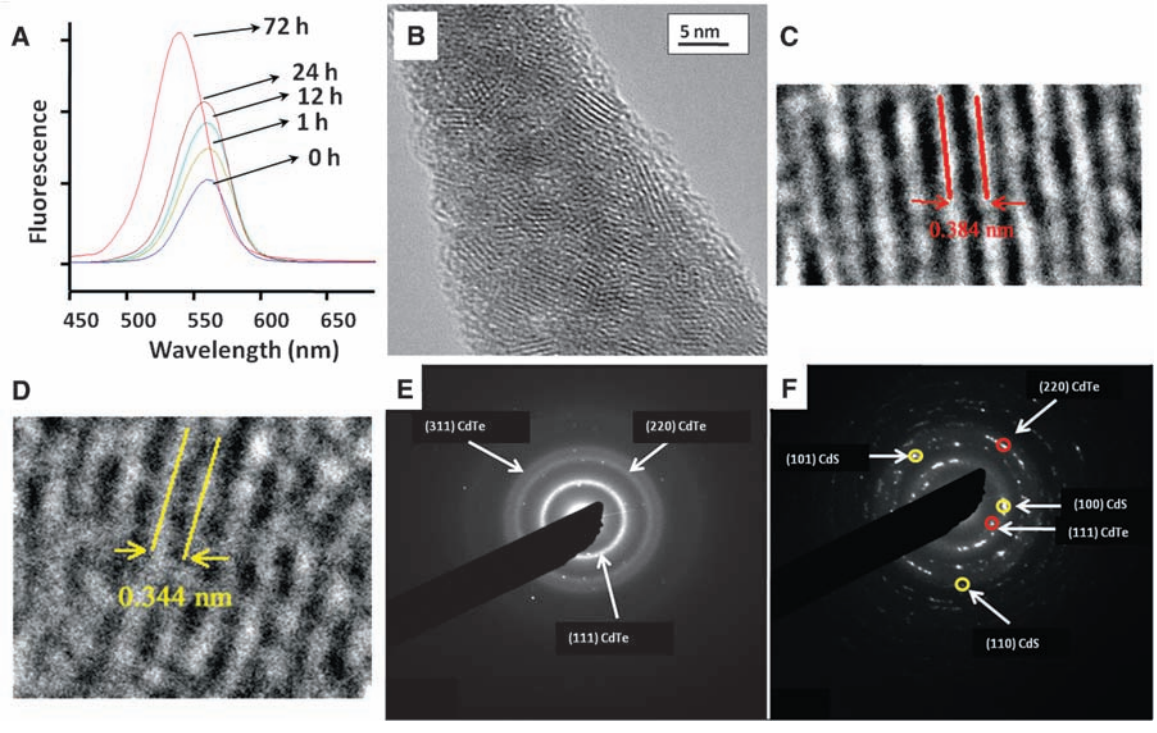

Fig. 2. (**A**) Evolution of fluorescence spectra for the self-organization of NPs into TRs. (**B**) HRTEM images for CdTe TRs taken in the "twist region." (**C** and **D**) Lattice fringes for {111} planes for the as-prepared NPs (C) and those in TR (D). (**E** and **F**) SAED patterns from CdTe NPs (E) and TR (F) with diffraction rings characterizing CdTe and CdS marked in red and yellow, respectively.

particle self-organization with corresponding trends in atomic composition. Both CdTe and CdS are light-sensitive (*12*), so subsequent studies were carried out both in dark and light conditions.

Examination of 1, 12, 24, and 72 hours time points of samples assembled under ambient light by scanning electron microscopy (SEM) and TEM revealed an interesting evolution of shapes of the multiparticle assemblies. Small spherical agglomerates were the starting point of the NP-to-TR transition and were exclusively present at the 1-hour time point after redispersion. By 12 hours, they transformed into much larger spheroids with complex elongated shapes (Fig. 3A) and then evolved into dog-bone–shaped NP systems by 24 hours (Fig. 3B). At 48 hours from the beginning of the self-assembly process, the dog-bone agglomerates reorganized themselves by stretching along a specific axis, resulting in fairly thick NWs (Fig. 3C) (*13*). At 72 hours, the thicker linear assemblies lead to thinner ones: On closer examination, they were the bunches of NWs or ribbons that unravel as "bouquets" of TRs of the same chirality (Fig. 3D and fig. S2) (*7*). The transition of spherical agglomerates to dog-bone–shaped assemblies is associated with a drastic reduction of Te content, which subsequently increased only slightly.

When the concentration of NPs was reduced from the beginning of the reaction, the dog-bone stage disappeared, individual nanoribbons were formed as an intermediate stage, and the TRs emerged at ~24 hours, followed by their bundling together at 72 hours (fig. S4) (*7*). These results indicated that ribbons represent an important intermediate product of the NP-to-TR transition, regardless of whether they are individual or associated into bunches.

When assembly takes place in the dark, after 1 hour, the NPs form loosely associated agglomerates that, again, exhibit a tendency to consolidate by 12 hours (Fig. 3E). No intermediate dog-bone–shaped structures were observed; their presence must be associated with a larger number of more strongly interacting particles. Instead, the NPs transformed into straight, multiparticle ribbons in 24 hours, which were also bunched together (Fig. 3F). These ribbons exhibited the propensity to debundle and become thinner after 48 hours (Fig. 3G). Eventually, the reaction in the dark resulted in distinct long, straight ribbons (Fig. 3H) in 72 hours with no twisting, which confirmed the importance of (i) straight ribbons as an intermediate stage and (ii) light as a stimulus for the transition of straight ribbons into twisted ones. It also offered a new means of control over helical NP assemblies.

XEDS data (Fig. 3, A to H, and fig. S6) (*7*) for all of the complex intermediate stages in both light and dark conditions reveal important points about the nature of the processes taking place and the origin of the unusual twisted morphology. The oxidation of Te^{2-} takes place in both light and dark. After 24 hours (i.e., at the dog-bone stage for light and the bunched-nanoribbons stage for dark conditions), the NPs are predominantly made from CdS, with only 3 to 5% of Te atoms. The amount of S in illuminated samples is consistently lower than that in NPs made in dark, and photocorrosion of CdS must be associated with the appearance of the twisted geometry. The conclusion can also be confirmed by the larger {111} lattice spacing observed in the assemblies obtained in light conditions, rather than in the dark (fig. S13) (*7*). Photooxidation of Te^{2-} leads to the strong change of chemical make-up of the NPs and accompanies the general assembly in ribbons, but it alone cannot be responsible for the appearance of helical assemblies.

The photooxidation of CdS in CdS/CdTe NPs before the complete removal of Te^{2-} centers may seem counterintuitive. However, the particles assembling into the ribbons and undergoing the twisting process are primarily made from CdS already (95 to 97%). The preference for oxidation of CdS over CdTe originates most likely from the gradient core-shell structure of the NPs obtained by the replacement of Te with S during the Te^{2-}

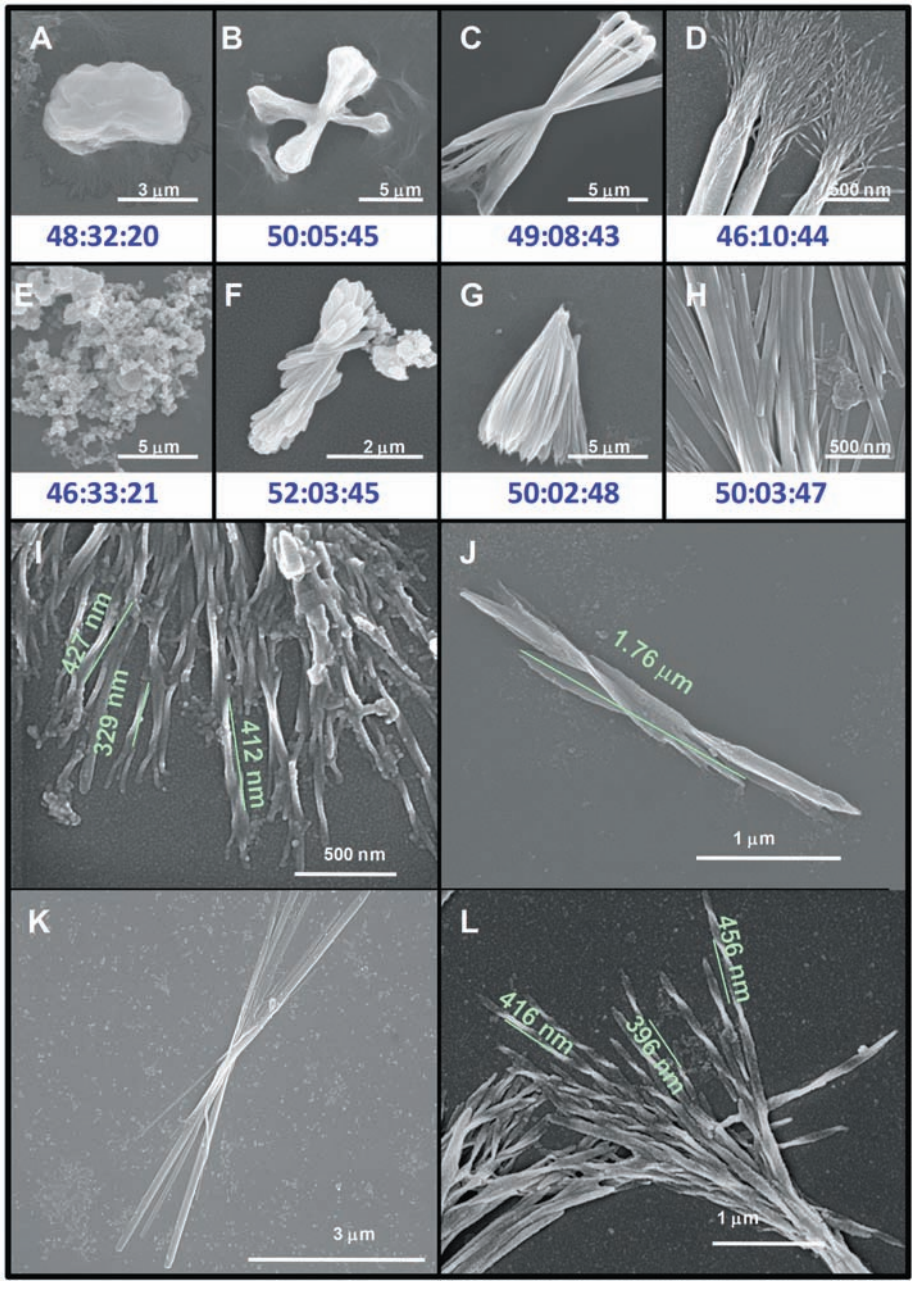

Fig. 3. Intermediate stages of TR formation and control of the twisting pitch. (**A** to **H**) SEM images of the ribbons assembled in ambient light (A) 12, (B) 24, (C) 48, and (D) 72 hours after redispersion of stabilizer-depleted particles. The ribbons assembled in dark conditions at the same time points: (E) 12, (F) 24, (G) 48, and (H) 72 hours. The XEDS Cd:Te:S atomic ratios for the particle assemblies are given below the corresponding images. (**I** and **J**) TRs prepared at different light intensities: (I) 61 and (J) 21 μW. (**K** and **L**) SEM images of ribbons after 52 hours in dark assembly (K) and then illuminated by the ambient light (61 μW) for 24 hours (L). NP concentration, 5 μM.

oxidation stage (*7*). SAED patterns indicate the presence of both CdTe and CdS phases (Fig. 2F), consistent with core-shell morphology. The surface of the NPs is likely to be pure CdS, whereas the Te atoms concentrated in the core become shielded from the photoreaction with dissolved oxygen. Also, the areas of delocalization of hole and electron tend to separate in NPs with CdTe/CdS heterojunctions, increasing the probability of interfacial photocorrosion.

We further explored the effects of illumination on NP-to-TR transitions. As such, TRs (~50 nm wide) prepared under 61 (ambient), 45, 38, and 21 μW showed pitch lengths of ~250 to 400 (Fig. 3I), ~500 to 600, ~1000, and ~1500 nm (Fig. 3J), respectively (fig. S7) (*7*). At all light intensities, HRTEM demonstrated the same polycrystalline nature composed of CdTe/CdS NPs. The dependence of the pitch length of TRs on light can also be traced in the dose of photons. A sample was aged in dark conditions for more than 2 days to form straight ribbons (Fig. 3K) and then was illuminated by ambient light (61 μW). The SEM images showed sequential change, and the pitch length was ~400-nm pitch length after 24 hours in light conditions (Fig. 3L).

The series of transformations of NPs and the subsequent structures observed are different from the reactions reported in previous organic or inorganic helical systems (*14*) or other NP assemblies (*15*, *16*). This necessitates gaining further insight into the balance of forces behind the TR formation. Typical helical structures originate from either specific crystal lattice distortions (*17*), mechanical strains (*18*), or chiral building blocks and form directly from the constituents. Helical structures can be formed because of mechanical stress or mismatch of the crystal lattice planes. The truncated tetrahedral structures of cubic II-VI semiconductor NPs can potentially be chiral, but we obtained no experimental evidence for chirality of individual NP involved in the NP-to-TR transition. The polycrystalline nature and the existence of two distinct crystalline phases in the TRs (CdTe and CdS) made the possibility of oriented attachment (*19*) and screw axis dislocations (*20*) in the extended crystal lattice as sources of helicity highly unlikely. Moreover, both of these mechanisms of helix formation at the nanoscale typically result in much shorter (by one to two orders of magnitude) pitch lengths than those observed in Fig. 1.

Therefore, we propose the following model for TR formation: Initially, between 1 and 24 hours, in both light and dark conditions, the attraction between the NPs is relatively weak, and dynamic aggregates with fairly spherical shapes are produced (Fig. 3, A and E). The same period of time overlaps with the completion of Te replacement with CdS. This change to CdS-dominant NPs prevents them from recrystallizing into CdTe thin, cylindrical NWs that have been observed before (*6*), because CdS has a greater activation barrier of recrystallization (*6*).

The forces between NPs are substantially stronger for light conditions, and the spheroids are larger and denser (Fig. 3A) than in dark conditions. We hypothesize that the multiparticle spheroids evolve into the dog-bone–shaped structures (Fig. 3B) because of gradual increase of anisotropic dipolar NP-NP interactions and the tendency of electric dipoles to align (*6*). The thin center part of the dog-bone and its conical apexes pointing to each other from each "pole" form through NP reorganization caused by forces that favor axial distribution. The potential origins of the greater dipolar interactions in the illuminated NPs are the entrapment of photogenerated charges at the interfacial states and unequal photoetching, which increases the value of the dipole moment (*21*). The reorganization continues until the round "clouds" become separated and eventually reorganize by stretching and producing ribbons and their bundles (Fig. 3, C and D).

Unlike the initial round agglomerates, the layers of NPs in the ribbons are well connected to each other (Fig. 2B) by short-range van der Waals interactions and hydrophilic or hydrophobic, dipole-dipole, and charge-dipole forces. In such objects, twisting can be produced as a result of internal shear strain between different NP layers, which can be partially relieved by acquiring the helical shape with uniform pitch length, despite some increase of elastic energy stored in the ribbon as a whole upon twisting. This is a common property of many ribbon-like structures (*22*) and was also observed in ribbons from multiwalled carbon nanotubes that acquire a twisted conformation to gain better registry between interacting graphene sheets (*23*). The source of internal strain in our ribbons is light-induced photocorrosion (*24*, *25*) of individual NP units, which results in reorganization of the bonded NPs trying to attain better and/or different packing because of the change of charge and/or dipole moment.

In the dark, no strain is generated, and the ribbons remain straight (Fig. 3, H and K) but tend to bunch. When light is on, photocorrosion of CdS results in the increase of charge/dipole in the already assembled ribbons, the stress between the layers of NPs gradually builds up with increasing the time or intensity of illumination, and twisting occurs. A greater degree of photoetching results in greater strain in the ribbons, and hence, stronger twisting (Fig. 3, I and J). The overall dose of illumination is most important in this respect; thus, the twisting can be controlled by both intensity (Fig. 3, I and J) and the time of light exposure (Fig. 3L).

Different experimental results, such as TEM/SEM images, XEDS, x-ray photoelectron spectroscopy (XPS), and dynamic light scattering data (Figs. 1 to 3) (*7*) support this mechanism of NP assembly into TRs. Changes in atomic percent composition seen in XEDS (Fig. 3, A to H, and fig. S6) (*7*) and XPS data (figs. S8 to S11) (*7*) confirmed photoinduced oxidation of CdS. There are two additional pieces of evidence for this mechanism that are particularly revealing. The key role of oxidation in TR formation can be confirmed by performing the NP self-organization reaction in an inert atmosphere. Even under light, no twisting was observed (fig. S12) (*7*) when oxygen was excluded from the reaction. Additionally, the steady increase of the zeta potential of NPs (fig. S15) from –10 to –50 mV clearly indicated that photoreaction results in a great increase in particle charge. This finding confirms the generation of a strong long-distance strain in the ribbons upon illumination. Alternatively, chemical oxidation with H_2O_2 fails to generate high zeta potential (always below –25 mV and eventually drops to zero) and, thus, fails to produce TRs (fig. S18) (*7*).

To further understand the assembly process, we carried out computer simulations to ascertain why the NPs under these conditions produce ribbons as the key precursors to TRs in light and dark conditions, and not chains (*8*) or sheets (*1*), as previously found for the same NPs under different conditions. This is also important from the perspective of understanding and controlling the forces between the NPs, so that the design of twisted and other self-organized microstructures can be done at the NP level. To describe the self-organization process of NPs, we used the same coarse-grained simulation model as did Tang *et al*. and Zhang *et al*. (*1*, *8*, *26*), with

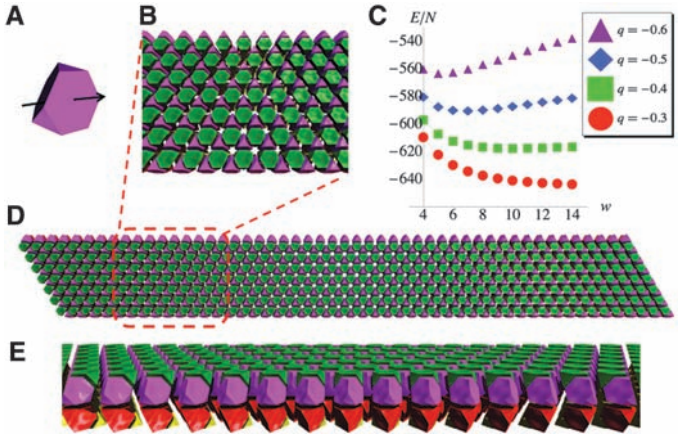

Fig. 4. (**A**) A truncated tetrahedron particle used in the simulations. (**B**) Close-up of the hexagonal packing structure obtained from BUBBA. (**C**) Plot of the energy per particle (*E*/*N*) measured in kilojoules per mole versus the width (*w*) of a ribbon measured in particles. (**D** and **E**) Top and side views, respectively, of straight ribbons. Pink and yellow tetrahedra point up; green and red tetrahedra point down. The arrow indicates the direction of the dipole moment.

modified parameters (*7*) to account for the present experimental conditions. Our choice of parameters reflects the reduced amount of TGA per CdTe, resulting in a net decrease of the charge, an increase of the face-face attraction energy, and a change in the direction of the dipole moment as compared with the conditions under which chains are obtained.

We used a recently developed technique for predicting ordered assemblies of building blocks with strong interactions via bottom-up building block assembly (BUBBA) (*26*) to determine the preferred local packing structure of tetrahedrons within ribbons. Then, Monte Carlo simulations were used to calculate the energy as a function of ribbon width to ascertain whether, and under what conditions, ribbons of finite width (rather than chains or sheets) (*1*, *8*) were the minimum energy structures. We found that NPs form four interdigitated layers grouped in two bilayers with tetrahedrons arranged hexagonally and inverted in alternate layers for denser packing (Fig. 4), which is consistent with TEM and SEM observations (Figs. 1, G to I, and 2B), albeit without the packing perfection seen in the simulations. The energy of the ribbon is minimized for a range of widths of ~18 to 110 nm, which matches structural parameters of TRs very well (Figs. 1 to 3). Increasing the charge resulted in more narrow ribbons, whereas decreasing the charge resulted in wider ribbons.

Overall, the multiparticle behavior and transition from packing into chains, ribbons, and sheets can be understood in terms of a competition between the face-face attraction and the charge-charge repulsion. For low charge and strong face attraction, as was the case in previous studies (*1*), particles pack very densely and would, if constrained to the same packing structure, form infinite two-dimensional sheets. By increasing the amount of charge, an infinite sheet becomes energetically unfavorable because of the long-range electrostatic repulsion, and NPs assemble as ribbons. Further increase of particle charge will eventually result in chains, as was observed for higher concentrations of TGA (*6*, *8*). Note that this concerns the effect of NP charge before the assembly. Once a larger NP system is assembled and held together by strong interparticle interactions, it may not be able to transition freely from sheets to ribbons of smaller width and then to chains. However, if there are structural units more loosely attached to each other, such as ribbons in bunches, they do separate, as can be seen by the unraveling of the bouquets of TRs (Fig. 3D and fig. S14).

The notion of evolving NP assemblies and better understanding of parameters controlling behavior of large numbers of nanoscale particles as a whole will be useful for many other nanocolloid systems. This study demonstrates that light can induce microscale twisting of the matter due to strong effect on the mutual interactions of nanoscale building blocks in a multibody system. The modulation in the pitch length for the TRs under different light intensities creates a new approach in the synthesis of nanostructures and new opportunities to generate nanomaterials with controlled circular dichroism and other optical, electronic, and mechanical properties.

References and Notes

1. Z. Tang, Z. Zhang, Y. Wang, S. C. Glotzer, N. A. Kotov, *Science* **314**, 274 (2006).
2. R. S. Yang, Z. L. Wang, *J. Am. Chem. Soc.* **128**, 1466 (2006).
3. S. C. Glotzer, M. J. Solomon, N. A. Kotov, *AIChE J.* **50**, 2978 (2004).
4. S. C. Glotzer, M. J. Solomon, *Nat. Mater.* **6**, 557 (2007).
5. C. Li, N. Murase, *Chem. Lett.* **34**, 92 (2005).
6. Z. Tang, N. A. Kotov, M. Giersig, *Science* **297**, 237 (2002).
7. See supporting material on *Science* Online.
8. Z. Zhang, Z. Tang, N. A. Kotov, S. C. Glotzer, *Nano Lett.* **7**, 1670 (2007).
9. W. W. Yu, L. H. Qu, W. Z. Guo, X. G. Peng, *Chem. Mater.* **15**, 2854 (2003).
10. J. Guo, W. Yang, C. Wang, *J. Phys. Chem. B* **109**, 17467 (2005).
11. K. V. K. Rao, S. V. N. Naidu, L. Iyengar, *J. Am. Ceram. Soc.* **51**, 467 (1968).
12. M. T. S. Nair, P. K. Nair, R. A. Zingaro, E. A. Meyers, *J. Appl. Phys.* **75**, 1557 (1994).
13. S. Busch *et al.*, *Eur. J. Inorg. Chem.* **1999**, 1643 (1999).
14. M. J. Bierman, Y. K. A. Lau, A. V. Kvit, A. L. Schmitt, S. Jin, *Science* **320**, 1060 (2008); published online 1 May 2008 (10.1126/science.1157131).
15. Y. Zhou, Q. M. Ji, M. Masuda, S. Kamiya, T. Shimizu, *Chem. Mater.* **18**, 403 (2006).
16. T. Vossmeyer *et al.*, *Science* **267**, 1476 (1995).
17. K. S. Cho, D. V. Talapin, W. Gaschler, C. B. Murray, *J. Am. Chem. Soc.* **127**, 7140 (2005).
18. L. S. Li, H. Z. Jiang, B. W. Messmore, S. R. Bull, S. I. Stupp, *Angew. Chem. Int. Ed.* **46**, 5873 (2007).
19. D. V. Talapin, H. Yu, E. V. Shevchenko, A. Lobo, C. B. Murray, *J. Phys. Chem. C* **111**, 14049 (2007).
20. X. D. Han *et al.*, *Nano Lett.* **7**, 452 (2007).
21. Y. Wang, Z. Tang, M. A. Correa-Duarte, L. M. Liz-Marzán, N. A. Kotov, *J. Am. Chem. Soc.* **125**, 2830 (2003).
22. T. McMillen, A. Goriely, *J. Nonlinear Sci. E* **12**, 241 (2002).
23. M.-F. Yu *et al.*, *Phys. Rev. B* **64**, 241403 (2001).
24. S. Yang *et al.*, *J. Am. Chem. Soc.* **128**, 10460 (2006).
25. A. Goriely, P. Shipman, *Phys. Rev. E* **61**, 4508 (2000).
26. E. Jankowski, S. C. Glotzer, *J. Chem. Phys.* **131**, 104104 (2009).

27. We acknowledge joint financial support by the Air Force Office of Scientific Research under Multiuniversity Research Initiative grant FA9550-06-1-0337. P.P. thanks the Fannie and John Hertz Foundation for support of his work through a graduate fellowship. This research was supported by the World Class University program through the Korea Science and Engineering Foundation funded by the Ministry of Education, Science and Technology (grant R33-2008-000-10021-0). We thank J. Kim (Univ. of Michigan) for helpful suggestions and discussions and W. Chen (JiangNan University) for assistance with some TEM data. P.P.'s work at the Center for Nanoscale Materials was supported by the Office of Science, Office of Basic Energy Sciences, of the U.S. Department of Energy under contract no. DE-AC02-06CH11357. P.P. acknowledges the support of the Willard Frank Libby postdoctoral fellowship from Argonne National Laboratory. The transmission electron microscope used in the study was supported by NSF grant DMR-9871177, and the scanning electron microscope used was supported by NSF grant DMR-0320740. S.C.G. and A.S. acknowledge the support of the J. S. McDonnell Foundation for the development of BUBBA. K.C. thanks Marie Curie Actions MOIF-CT-2006-039636 for financial support.

Supporting Online Material

www.sciencemag.org/cgi/content/full/science.1177218/DC1
Materials and Methods
SOM Text
Figs. S1 to S22
References

3 June 2009; accepted 2 February 2010
Published online 11 February 2010;
10.1126/science.1177218
Include this information when citing this paper.

The Near-Tip Fields of Fast Cracks

Ariel Livne, Eran Bouchbinder,* Ilya Svetlizky, Jay Fineberg†

In a stressed body, crack propagation is the main vehicle for material failure. Cracks create large stress amplification at their tips, leading to large material deformation. The material response within this highly deformed region will determine its mode of failure. Despite its great importance, we have only a limited knowledge of the structure of this region, because it is generally experimentally intractable. By using a brittle neo-Hookean material, we overcame this barrier and performed direct and precise measurements of the near-tip structure of rapid cracks. These experiments reveal a hierarchy of linear and nonlinear elastic zones through which energy is transported before being dissipated at a crack's tip. This result provides a comprehensive picture of how remotely applied forces drive material failure in the most fundamental of fracture states: straight, rapidly moving cracks.

Material failure occurs at small scales in the immediate vicinity of the tip of a crack. The existence of a crack in an otherwise perfect material dramatically amplifies applied stresses to values that approach a mathematical singularity at the crack's tip (*1*). The stress fields formed by a crack transport remotely applied elastic energy to the crack's tip, where the energy is dissipated by material fracture. Even small external stresses can generate sufficiently large stresses within this small microscopic region to initiate fracture. Linear elastic fracture mechanics (LEFM) provides the theoretical framework for understanding this stress amplification. LEFM assumes that the material under stress obeys linear elasticity (that is, Hooke's law) at every point up to the very near vicinity of a crack's tip. All of the complex dissipative and nonlinear processes that are involved in fracture and not described by LEFM are assumed to occur within a sufficiently small region around the tip. Nevertheless, this

Racah Institute of Physics, Hebrew University of Jerusalem, Jerusalem 91904, Israel.

*Present address: Department of Chemical Physics, Weizmann Institute of Science, Rehovot 76100, Israel.
†To whom correspondence should be addressed. E-mail: jay@vms.huji.ac.il